Double-folding model for heavy-ion optical potential: Revised and applied to study ^{12}C and ^{16}O elastic scattering

Dao T. Khoa,* W. von Oertzen, and H. G. Bohlen
Bereich Schwerionenphysik, Hahn-Meitner-Institut-GmbH, Glienicker Strasse 100, D-14109 Berlin, Germany
(Received 26 October 1993)

The double-folding model is generalized for the calculation of the nucleus-nucleus potential using the new version of the density-dependent M3Y interaction which reproduces consistently the equilibrium density, and binding energy of normal nuclear matter as well as the density- and energy dependence of the nucleon optical potential. The exchange part of the heavy-ion optical potential is evaluated within a local density formalism, using the finite-range exchange components of the same interaction. The model is used successfully to describe the elastic ^{12}C and ^{16}O scattering data at low and medium energies. The influence of different density-dependent parameters (which determine different nuclear equations of state) on the description of heavy-ion scattering is also discussed.

PACS number(s): 24.10.Ht, 21.30.+y, 21.65.+f, 25.70.Bc

I. INTRODUCTION

During the last decade, the double-folding model [1] has been widely used by many groups in describing the heavy-ion (HI) scattering, due to its simple handling in numerical calculations. The original version of the folding model [1] seems to deliver satisfying results in most cases where the HI interaction is dominated by strong absorption, i.e., when the elastic-scattering data are sensitive to the HI optical potential only in the surface region. However, it is well established now that in certain cases of nuclear rainbow scattering, observed first for α particles [2] and later on for other light HI systems [3–5], where the data are sensitive to the HI optical potential over a wider radial domain, the simple double-folding model [1] failed to give a good description to the data. Therefore, some further developments of the folding model have been made to obtain a more realistic shape of the folded potential. One of these approaches is to impose on the widely used M3Y effective nucleon-nucleon (NN) interaction [6] an explicit density dependence to account effectively for the in-medium effects which are more substantial at small internuclear distances, the so-called DDM3Y interaction [7]. Another way is to correctly treat the single nucleon knock-on exchange (SNE) effects arising from the Pauli principle [8,9] where the intrinsic energy and density dependence of the HI potential due to the antisymmetrization effects is taken into account correctly. In this approach the exchange potential is derived from first principles within a local density formalism, using the *finite-range* exchange (M3Y/FRE) interaction, which is essentially a much better approximation as compared to the *zero-range* pseudopotential [10] adopted in the usual double-folding calculations [1,7].

Even though these improved versions of the folding model have been used quite successfully to calculate the α-nucleus and nucleus-nucleus potentials, there remains an important question of how good the M3Y interaction approximates the NN interaction in a nuclear medium. A foremost requirement for an effective in-medium NN interaction is that the interaction must correctly reproduce the basic properties of the normal nuclear matter. Our recent nuclear matter study [11] using the M3Y interaction has shown that both the original M3Y interaction [6] and its density-dependent version DDM3Y [7] cannot provide a reasonable description of the normal nuclear matter. Therefore, some new density-dependent versions of the M3Y interaction have been introduced [11] which consistently reproduce the basic nuclear matter properties as well as the density and energy dependence of the nucleon optical potential. While giving the same description of the normal nuclear matter, the new density-dependent interactions generate different binding energies of the cold nuclear matter at higher densities, i.e., different equations of state (EOS) of the cold nuclear matter. In the present work the double-folding model is generalized, in the spirit of previous approaches [7–9], to calculate the real HI optical potential using the new density-dependent versions of the M3Y interaction [11] with the *local* exchange part evaluated exactly. The reliability of our approach is tested in the detailed folding analyses of the elastic-scattering data for ^{12}C and ^{16}O at low and medium energies. The sensitivity of the results to different density dependences of the interaction favors the concept that the cold nuclear matter is most probably governed by a soft EOS.

A brief description of the new density-dependent interaction, the generalization of the double-folding model, and some details of the numerical calculation are given in Sec. II. In Sec. III the results of the folding analyses of the ^{12}C and ^{16}O elastic scattering data are discussed. Conclusions of the present paper are summarized in Sec. IV.

*Electronic address: khoa@vax.hmi.d400.de

TABLE I. The parameters of different density dependences of the M3Y interaction [see Eqs. (3)]. The nuclear matter compressibilities K were obtained from the HF calculation reported in Ref. [11].

Interaction	$F(\rho)$	C	α	β	K (MeV)
DDM3Y1	Eq. (3a)	0.2845	3.6391	2.9605 fm^3	149.5
BDM3Y1	Eq. (3b)	1.2253	1.5124 fm^3	1.0	210.6
BDM3Y2	Eq. (3b)	1.0678	5.1069 fm^6	2.0	332.1
BDM3Y3	Eq. (3b)	1.0153	21.073 fm^9	3.0	453.6

II. THEORETICAL FORMALISM

A. Effective density-dependent NN interaction

To evaluate an in-medium NN interaction starting from a realistic free NN interaction still remains a challenge for the nuclear many-body theory. The sophisticated Brueckner-Hartree-Fock (BHF) calculations which include the two- and three-nucleon correlations are still unable to describe simultaneously the equilibrium density and the binding energy of the normal nuclear matter, and the inclusion of higher-order correlations as well as relativistic effects is shown to improve the situation [12]. Therefore, most of the *microscopic* nuclear reaction calculations so far still use different kinds of effective in-medium NN interaction. Such interactions can be roughly divided into two groups. In the first group one parametrizes the effective interaction directly as a whole (e.g., the Skyrme forces), leaving out any connection with a realistic free NN interaction. In the second group one first derives the effective interaction in the lowest-order of the many-body calculation (a solution of the Bethe-Goldstone equation), starting from a realistic NN interaction which reproduces the free NN scattering data; the higher-order corrections are then parametrized (mostly in terms of a density and momentum dependence) and included into the interaction so that already in a simple Hartree-Fock (HF) calculation one obtains a good description of the normal nuclear matter. We have constructed [11], within the second scheme, an energy- and density-dependent effective interaction which is based on the original M3Y interaction as the first-order effective interaction. Since the original M3Y interaction [6] was derived by fitting its matrix elements in an oscillator basis to those elements of the G matrix obtained from a Bethe-Goldstone calculation using the Reid soft-core NN interaction, our nuclear matter results [11] obtained in a HF calculation might be compared to those of a sophisticated BHF calculation with the higher-order corrections taken into account. With the direct (v_D) and exchange ($v_{\rm EX}$) parts of the original interaction determined from the singlet and triplet even ($v_{\rm SE}, v_{\rm TE}$) and odd ($v_{\rm SO}, v_{\rm TO}$) components of the M3Y forces [6]

$$v_D(r) = 7999.0\frac{\exp(-4r)}{4r} - 2134.25\frac{\exp(-2.5r)}{2.5r}, \quad \text{(1a)}$$

$$v_{\rm EX}(r) = 4631.38\frac{\exp(-4r)}{4r} - 1787.13\frac{\exp(-2.5r)}{2.5r} - 7.8474\frac{\exp(-0.7072r)}{0.7072r}, \quad \text{(1b)}$$

we have parametrized [11] the energy- and density-dependent M3Y interaction in the form

$$v_{D(\rm EX)}(\rho, E, r) = F(\rho)g(E)v_{D(\rm EX)}(r),$$

$$g(E) = 1 - 0.002E. \quad (2)$$

The explicit form of the density-dependent factor $F(\rho)$ is introduced as

$$F(\rho) = \begin{cases} C[1 + \alpha\exp(-\beta\rho)], & \text{the DDM3Y-type,} \quad \text{(3a)} \\ C(1 - \alpha\rho^{\beta}), & \text{the BDM3Y-type.} \quad \text{(3b)} \end{cases}$$

The parameters in Eqs. (3) are adjusted [11] to reproduce the basic properties of the normal nuclear matter while generating different EOS for the cold nuclear matter (see Table I and Fig. 1). The energy-dependent factor $g(E)$ in Eq. (2) is introduced [11] to account for an additional (explicit) energy dependence of the NN interaction which is absent in the original static M3Y interaction. Note that the parameters of the well-known DDM3Y interaction [7] were only fitted to the density and energy dependence of the microscopic nucleon optical potential obtained by Jeukenne, Lejeune, and Mahaux (JLM) [13], and they turned out to be irrelevant in describing the saturation of the cold nuclear matter [11]. The new parametrizations (Table I) used in the present paper give both a good description of the normal nuclear matter and an agreement with the JLM results for the nucleon optical potential (see Figs. 1–3 of Ref. [11]) at different energies and densities.

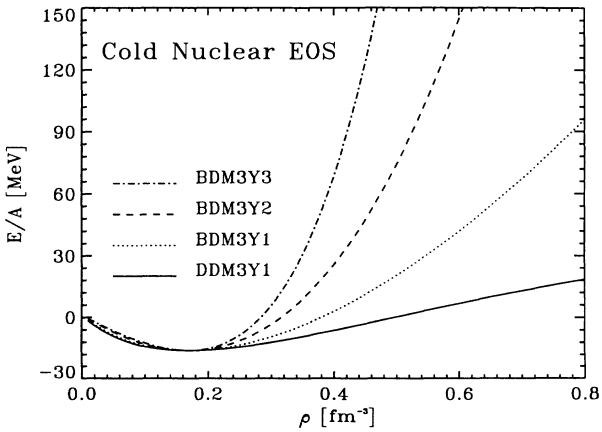

FIG. 1. Different nuclear EOS generated by different-density dependent versions of the M3Y interaction [see Eqs. (3)] with parameters giving the nuclear compressibilities $K \simeq 150$–454 MeV (Table I).

B. Generalized double-folding model

The basis of the folding approach has been presented in detail by Satchler and Love [1]. We give here only a short description of the model and concentrate more on its improved version being used in the present paper. In the first order of the many-body theory, the microscopic nucleus-nucleus potential can be evaluated as an antisymmetrized HF-type potential for the dinuclear system

$$V = V_D + V_{\rm EX} = \sum_{i\in A_1, j\in A_2} [\langle ij|v_D|ij\rangle + \langle ij|v_{\rm EX}|ji\rangle], \quad (4)$$

where $|i\rangle$ and $|j\rangle$ refer to the single-particle wave functions of nucleons in the two colliding nuclei A_1 and A_2, respectively; v_D and $v_{\rm EX}$ are the direct and exchange parts of the effective NN interaction considered in Sec. II A. By introducing the one-body density matrices $\rho_{1(2)}(\mathbf{r},\mathbf{r}')$ of the two colliding nuclei [8,9] [with the diagonal terms giving the matter densities $\rho(\mathbf{r},\mathbf{r}) \equiv \rho(\mathbf{r})$], one can explicitly write the energy-dependent direct and exchange potentials as

$$V_D(E,\mathbf{R}) = \int \rho_1(\mathbf{r}_1)\rho_2(\mathbf{r}_2)v_D(\rho,E,s)d\mathbf{r}_1 d\mathbf{r}_2, \quad \text{with } \mathbf{s} = \mathbf{r}_2 - \mathbf{r}_1 + \mathbf{R}, \quad (5)$$

$$V_{\rm EX}(E,\mathbf{R}) = \int \rho_1(\mathbf{r}_1,\mathbf{r}_1+\mathbf{s})\rho_2(\mathbf{r}_2,\mathbf{r}_2-\mathbf{s})v_{\rm EX}(\rho,E,s) \times \exp\left[\frac{i\mathbf{k}(\mathbf{R})\mathbf{s}}{M}\right] d\mathbf{r}_1 d\mathbf{r}_2. \quad (6)$$

Here $k(\mathbf{R})$ is the relative-motion momentum given by

$$k^2(\mathbf{R}) = \frac{2mM}{\hbar^2}[E_{\rm c.m.} - V(E,\mathbf{R}) - V_C(\mathbf{R})], \quad (7)$$

where $M = A_1A_2/(A_1+A_2)$ is the reduced mass, $E_{\rm c.m.}$ the center-of-mass (c.m.) energy, E the incident laboratory energy per nucleon, and m the bare nucleon mass. $V(E,\mathbf{R}) = V_D(E,\mathbf{R}) + V_{\rm EX}(E,\mathbf{R})$ and $V_C(\mathbf{R})$ are the total nuclear and Coulomb potentials, respectively.

In the present work the direct potential (5) is evaluated using the same method as that developed by Kobos *et al.* [7] with some modification to also include the BDM3Y-type interaction (3b) in the calculation. Therefore, we give here only the details of the calculation scheme for the exchange part of the HI potential which is a generalization of the approaches suggested first in Refs. [8,9]. It can be seen from Eq. (6) that the energy-dependent HI potential is nonlocal through its exchange term. Since the exact treatment of the nonlocal exchange term is too complicated numerically, one usually obtains the equivalent local potential by using a realistic localized expression for the density matrix [14]

$$\rho(\mathbf{R},\mathbf{R}+\mathbf{s}) \simeq \rho\left(\mathbf{R}+\frac{\mathbf{s}}{2}\right)\hat{j}_1\left(k_F\left(\mathbf{R}+\frac{\mathbf{s}}{2}\right)s\right) \quad (8)$$

with

$$\hat{j}_1(x) = 3(\sin x - x\cos x)/x^3.$$

The average local Fermi momentum k_F is chosen [14] to accelerate the convergence of the density-matrix expansion and has the following form

$$k_F(\mathbf{r}) = \left\{\frac{5}{3\rho(\mathbf{r})}\left[\tau(\mathbf{r}) - \frac{1}{4}\nabla^2\rho(\mathbf{r})\right]\right\}^{1/2}. \quad (9)$$

Further, we choose the extended Thomas-Fermi approximation [15] for the kinetic energy density $\tau(\mathbf{r})$ and the local Fermi momentum can be obtained as

$$k_F(\mathbf{r}) = \left\{\left[\frac{3}{2}\pi^2\rho(\mathbf{r})\right]^{2/3} + \frac{5C_S[\nabla\rho(\mathbf{r})]^2}{3\rho^2(\mathbf{r})} + \frac{5\nabla^2\rho(\mathbf{r})}{36\rho(\mathbf{r})}\right\}^{1/2}, \quad (10)$$

where C_S is the strength of the so-called Weizsäcker term representing the surface contribution to $\tau(\mathbf{r})$. Normally one takes $C_S \simeq \frac{1}{36}$ for a finite fermionic system. However, a detailed study by Baltin [16] has shown that in a region of small density or high $\nabla\rho$ (which just corresponds to the nuclear surface) the Weizsäcker correction term to the kinetic energy density is much larger and should have a strength of $C_S \simeq \frac{1}{4}$. Therefore, as opposed to previous approaches [8,9], we have taken the latter value for C_S which turned out to also give a more realistic shape to our microscopic HI potential. For the infinite nuclear matter the surface correction term vanishes and one has k_F reduced to the Fermi momentum of the nuclear matter with density ρ which corresponds to the well-known Slater approximation for the nonlocal density matrix.

Another important step is to specify the overlap density which enters the expressions (3). We have taken this density to be the sum of the densities of the two colliding nuclei at the midpoint of the internucleon separation, i.e.,

$$F(\rho) = F\left[\rho_1\left(\mathbf{r}_1+\frac{\mathbf{s}}{2}\right) + \rho_2\left(\mathbf{r}_2-\frac{\mathbf{s}}{2}\right)\right]. \quad (11)$$

This procedure simply corresponds to the local density approximation assumed in different nuclear matter studies [17] or the so-called frozen density approximation (FDA) usually adopted in the folding model [1,7,18]. Some more discussion on the validity of the FDA is given below, in Sec. III A.

After some transformations one can obtain the energy-dependent exchange potential in the following *local* form:

$$V_{\rm EX}(E,\mathbf{R}) = 4\pi g(E)\int_0^\infty v_{\rm EX}(s)s^2 ds j_0(k(\mathbf{R})s/M) \times \int f_1(\mathbf{r},s)f_2(\mathbf{r}-\mathbf{R},s) \times F[\rho_1(\mathbf{r})+\rho_2(\mathbf{r}-\mathbf{R})]d\mathbf{r}, \quad (12)$$

where

$$f_{1(2)}(\mathbf{r},s) = \rho_{1(2)}(\mathbf{r})\hat{j}_1\left(k_{F1(2)}(\mathbf{r})s\right)$$

and $j_0(x) = \sin x/x$. Applying the folding formulas in momentum space [1], one can deduce the exchange potential (12) to the form

$$V_{\rm EX}(E,R) = 4\pi g(E) \times \int_0^\infty G(R,s)j_0(k(R)s/M)v_{\rm EX}(s)s^2 ds, \quad (13)$$

where

$$G(R,s) = \frac{C}{2\pi}\int_0^\infty \left[h_1(t,s)h_2(t,s) + \alpha\overline{G(t,s)}\right] j_0(tR)t^2 dt, \quad (14)$$

and

$$h_{1(2)}(t,s) = 4\pi\int_0^\infty f_{1(2)}(r,s)j_0(tr)r^2 dr.$$

The explicit form of the $\overline{G(t,s)}$ function is determined by the explicit form of the density-dependent function $F(\rho)$, namely,

$$\overline{G(t,s)} = \begin{cases} y_1(t,s)y_2(t,s) & \text{for DDM3Y-type interaction;} \\ -\sum_{n=0}^{\beta}\binom{\beta}{n} z_1^{(\beta-n+1)}(t,s)z_2^{(n+1)}(t,s) & \text{for BDM3Y-type interaction.} \end{cases} \quad (15)$$

Here

$$y_{1(2)}(t,s) = 4\pi\int_0^\infty f_{1(2)}(r,s)\exp\left[-\beta\rho_{1(2)}(r)\right] \times j_0(tr)r^2 dr$$

and

$$z_{1(2)}^{(m)}(t,s) = 4\pi\int_0^\infty f_{1(2)}(r,s)\rho_{1(2)}^m(r)j_0(tr)r^2 dr.$$

Note that Eqs. (13) and (14) were obtained assuming an isotropic form for the densities of the nuclei (which is the case for the ground-state density). In general, by expanding the densities into multipoles, one can obtain not only (13) for the optical potential but also the HI inelastic form factors (different multipole components of the HI potential) [19].

Since the exchange potential contains the relative-motion momentum $k(R)$ which in turn depends on the total HI potential [see Eq. (7)], one has to solve a self-consistency problem to obtain the exchange part of the HI potential at each radial point. In general, this problem can be solved by using an iterative procedure as has been done first by Chaudhuri *et al.* [8]. In our earlier works [9,19,20] in this direction we have used a closed expression for the exchange potential obtained from a series expansion of the Bessel function $j_0(k(R)s/M)$. This method has been proven recently by Abele and Staudt [21] to give the same results as the iterative procedure down to the radius of about 2 fm (for the ^{16}O+^{16}O system) while at the smallest distances the exact iteration gives a potential more attractive than that obtained with the closure approximation. Therefore, we have chosen in the present paper the iterative method again to ensure the self-consistency at all the radial points, using $V_D(E,R)$ as the starting potential to enter $j_0(k(R)s/M)$ in the exchange integral (13). The number of iterations needed to obtain the exact self-consistent results for $V_{\rm EX}(E,R)$ is around 20 at the smallest radii and ranges from 3 to 5 at the surface region which indicates stronger exchange effects at small internuclear distances.

The microscopic energy-dependent HI optical potentials calculated within our approach are used further in the optical model (OM) analyses to describe the ^{12}C and ^{16}O elastic-scattering data at different incident energies. All the nuclear densities used in our folding calculations, if not otherwise specified, are taken as a Fermi distribution with parameters chosen [18] to reproduce the shell-model densities for the considered nuclei. Since the original M3Y interaction [6] is real, the calculated HI potentials are also real and enter the OM analyses as the real part of the HI optical potential. The imaginary part, as in most of the folding analyses, is taken in some phenomenological form with the parameters adjusted to give the best fit to the scattering data. We have assumed for simplicity the Woods-Saxon (WS) shape for the imaginary potential so that the HI optical potential in our OM analyses is

$$U(E,R) = N_R[V_D(E,R)+V_{\rm EX}(E,R)] - iW_V\left[1+\exp\left(\frac{R-R_V}{a_V}\right)\right]^{-1} + 4iW_D a_D\frac{d}{dR}\left[1+\exp\left(\frac{R-R_D}{a_D}\right)\right]^{-1}, \quad (16)$$

where the renormalization factor N_R together with the parameters of the imaginary potential are adjusted to obtain the best fit to the scattering data. The WS surface term in Eq. (16) (denoted further as WSD) is optional and added only in cases where it essentially improves the agreement with data. The Coulomb potential $V_C(R)$ used in the calculation of the exchange potential [see Eq. (7)] and in the OM analyses is generated by folding two uniform charge distributions [22] with the radii

taken from the electron scattering data for the considered nuclei. All the OM analyses were made using the nonrelativistic code PTOLEMY [23]. For the medium energy cases considered in Sec. III, the effective masses and incident energies were used (see Tables II and V) to give the relativistically corrected c.m. kinematics [24].

III. RESULTS AND DISCUSSIONS

A. General considerations

Since the parameters of different density dependences (Table I) of the M3Y interaction have been adjusted [11] to reproduce the basic properties of the cold nuclear matter at saturation density (ρ_0), all the calculated potentials have about the same strength and slope at the surface (see, e.g., the folded potentials calculated for the $^{16}O+^{16}O$ system at 250 MeV shown in Fig. 2) which corresponds to the small overlap or low-density region. The main difference between different types of the folded potential is showing up at small internuclear distances which correspond to the higher overlap density of the two colliding nuclei. Thus the BDM3Y3 interaction, chosen to generate a very hard EOS (Table I), is much more re-

TABLE II. The optical potential parameters used in our folding analyses of the elastic $^{12}C+^{12}C$ scattering data at E_{lab} = 112–1449 MeV with the imaginary potential assumed to have a volume WS shape [the first two terms in Eq. (16)].

Potential	N_R	$-J_R$ (MeV fm^3)	$\langle r_R^2\rangle^{1/2}$ (fm)	W_V (MeV)	R_V (fm)	a_V (fm)	σ_R (mb)	χ^2
$^{12}C+^{12}C$, E_{lab} = 112 MeV								
DDM3Y1	0.9954	336.6	3.7950	18.259	5.1753	0.6679	1393	15.8
BDM3Y1	1.0298	339.6	3.8029	18.123	5.2134	0.6563	1391	15.2
BDM3Y2	1.1198	348.5	3.8291	17.605	5.3385	0.6171	1383	13.5
BDM3Y3	0.9832	279.5	3.9015	15.305	5.4541	0.5949	1354	32.8
$^{12}C+^{12}C$, E_{lab}=126.7 MeV								
DDM3Y1	0.9873	330.9	3.7967	17.949	5.3708	0.5810	1350	10.0
BDM3Y1	1.0188	332.9	3.8047	17.960	5.3836	0.5790	1353	9.6
BDM3Y2	1.0981	338.6	3.8309	18.271	5.4031	0.5762	1363	9.3
BDM3Y3	0.9734	274.1	3.9036	17.443	5.3844	0.5722	1332	18.1
$^{12}C+^{12}C$, E_{lab} = 240 MeV								
DDM3Y1	0.9253	288.8	3.8110	28.649	5.0754	0.6394	1383	42.2
BDM3Y1	0.9569	291.1	3.8192	28.870	5.0918	0.6370	1388	43.1
BDM3Y2	1.0345	296.7	3.8460	29.929	5.1180	0.6317	1403	46.2
BDM3Y3	0.9477	247.9	3.9196	27.401	5.1378	0.6247	1374	46.1
$^{12}C+^{12}C$, E_{lab} = 300 MeV								
DDM3Y1	0.9307	279.7	3.8190	28.349	5.0461	0.6916	1413	23.2
BDM3Y1	0.9545	279.6	3.8274	27.747	5.0917	0.6827	1413	25.4
BDM3Y2	1.0120	279.4	3.8546	27.256	5.1503	0.6726	1419	30.7
BDM3Y3	1.0577	266.1	3.9285	25.412	5.2630	0.6572	1424	39.6
$^{12}C+^{12}C$, E_{lab} = 1016 MeV, Imag. WS (I) pot. (Effective lab. energy=994 MeV, ^{12}C mass=12.270)								
DDM3Y1	0.9212	181.4	3.9280	17.683	5.0714	0.8371	1199	18.1
BDM3Y1	0.9517	182.4	3.9376	16.966	5.1652	0.8210	1203	21.9
BDM3Y2	1.0300	185.3	3.9675	16.143	5.2726	0.8294	1231	38.6
BDM3Y3	1.1006	179.5	4.0451	17.186	5.2171	0.8253	1236	104.7
$^{12}C+^{12}C$, E_{lab} = 1016 MeV, Imag. WS (II) pot. (Effective lab. energy=994 MeV, ^{12}C mass=12.270)								
DDM3Y1	0.9572	188.5	3.9280	49.283	3.6925	0.8315	1060	8.8
BDM3Y1	0.9784	187.5	3.9376	49.809	3.6793	0.8314	1059	8.7
BDM3Y2	1.0251	184.5	3.9675	50.436	3.6569	0.8323	1056	8.6
BDM3Y3	1.0854	177.0	4.0451	50.009	3.6341	0.8376	1051	9.8
$^{12}C+^{12}C$, E_{lab} = 1449 MeV, Imag. WS (I) pot. (Effective lab. energy=1404 MeV, ^{12}C mass=12.382)								
DDM3Y1	0.9168	142.9	4.0055	12.255	5.4093	1.0054	1191	26.1
BDM3Y1	0.9376	142.1	4.0156	11.701	5.4810	1.0301	1210	27.1
BDM3Y2	0.9937	141.2	4.0464	10.363	5.7173	1.0531	1245	30.4
BDM3Y3	1.0978	141.1	4.1248	10.121	6.2735	1.0483	1259	40.7
$^{12}C+^{12}C$, E_{lab} = 1449 MeV, Imag. WS (II) pot. (Effective lab. energy=1404 MeV, ^{12}C mass=12.382)								
DDM3Y1	0.9551	148.9	4.0055	44.852	3.7350	0.7809	927	20.4
BDM3Y1	0.9732	147.5	4.0156	44.509	3.7333	0.7783	921	19.6
BDM3Y2	1.0163	144.4	4.0464	43.053	3.7411	0.7729	908	17.6
BDM3Y3	1.0873	139.8	4.1248	38.819	3.7793	0.7702	886	13.4

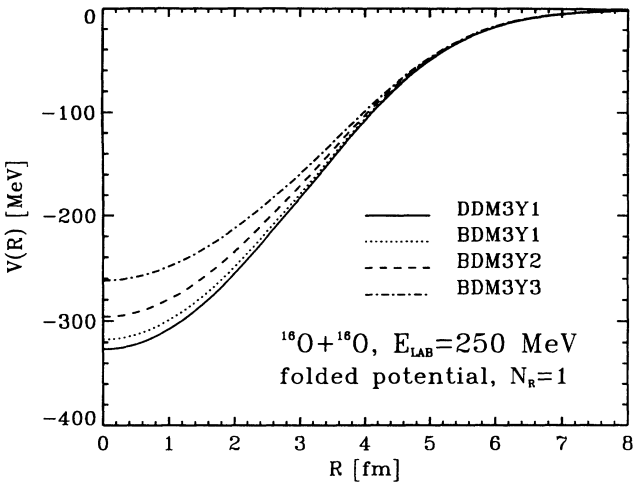

FIG. 2. The real folded potentials for the ^{16}O+^{16}O system at E_{lab} = 250 MeV calculated with different density-dependent versions of the M3Y interaction [see Eqs. (3)].

pulsive in the high-density region which in turn gives a folded potential less attractive than other folded potentials at small distances. To illustrate the high density which might be formed during a collision at different impact parameters we have plotted in Fig. 3 the results obtained for the ^{16}O+^{16}O system within the FDA (discussed in Sec. II B). One can see that at an internuclear distance from 2 to 3 fm the density should be well above the normal nuclear matter density, up to about $2\rho_0$. We note that this FDA is a reasonable approximation for the folding calculations [7,18] at energies not very low as compared to the Fermi energy. A more accurate picture of the dense nuclear matter formed during a HI collision can be given by some dynamical model. In Fig. 4 we have plotted the profile of the matter density built up during the ^{16}O+^{16}O collision at E_{lab} = 350 MeV and at the impact parameter of 2 fm, obtained from a calculation within the so-called quantum molecular dynamics approach [25] which has been proven quite successful in the dynamical simulation of HI collisions. One can see that during the compression stage, a dense matter with $\rho \sim 2\rho_0$ is formed in the center of the collision. Although

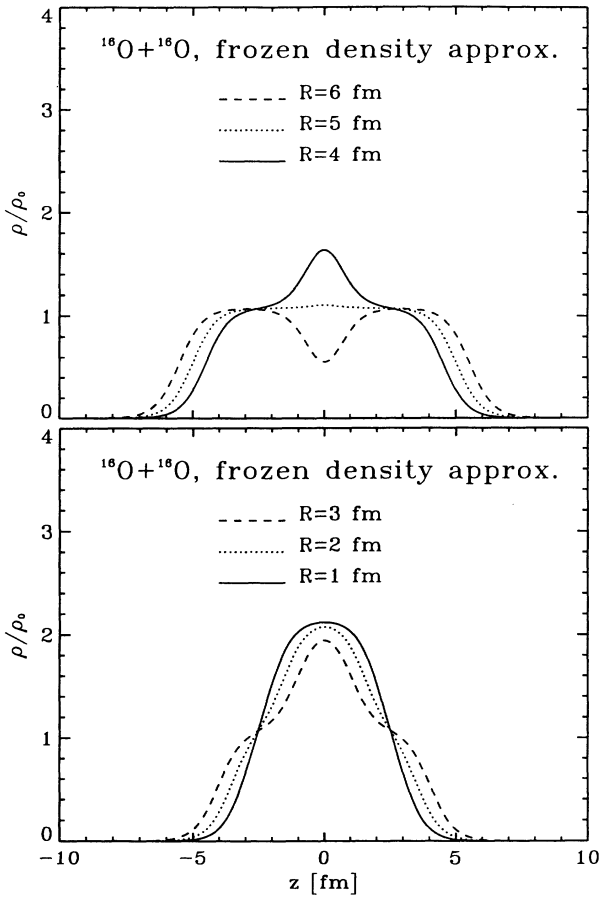

FIG. 3. The overlap density in the ^{16}O+^{16}O system at different internuclear distances (impact parameters) obtained within the FDA (see details in Sec. III A).

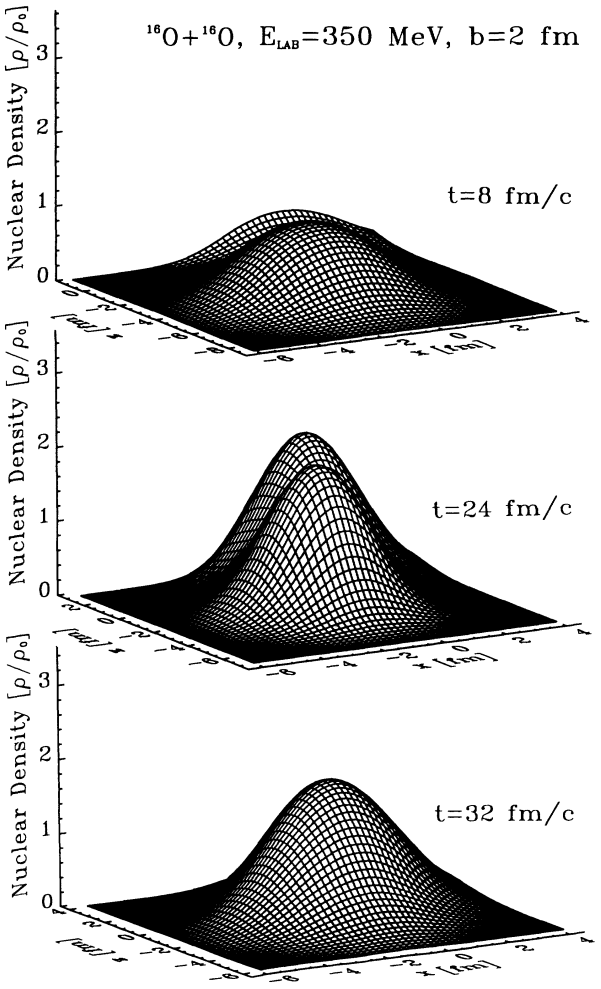

FIG. 4. The profile of the overlap density built up (at early times, t=8–32 fm/c) in the center of the ^{16}O+^{16}O collision at E_{lab} = 350 MeV and at impact parameter of 2 fm, given by the quantum molecular dynamics model [25].

one cannot simulate an elastic-scattering event from such a dynamical calculation, the results shown in Fig. 4 confirm to a certain extent the validity of the FDA used in the folding model. At very low energies, an adiabatic approximation might be more appropriate than the FDA and the formalism given in Sec. II as well as the simple approach developed in Ref. [7] should be modified accordingly.

The calculated potentials can be used in general to analyse all the available HI scattering data. However, the most interesting are those data which are sensitive to the HI potential not only at the surface region but also at smaller internuclear distances. They would allow us to extract from different density-dependent HI potentials the most realistic one, which in turn should be selective to the density dependence of the effective NN interaction, i.e., to some realistic type of the EOS of the cold nuclear matter. This is the main motive of our study and for that purpose we have analysed most of the available refractive scattering data measured so far with ^{12}C and ^{16}O.

Before going on to discuss the results of our analyses in detail, we emphasize that the exchange term of the HI potential arising from the SNE effects is treated explicitly in terms of a local exchange potential $V_{\rm EX}(E,R)$. From the discussion in Sec. II it becomes clear that the contribution of the $V_{\rm EX}$ to the total HI potential is energy- and density dependent. To show this effect we have plotted in Fig. 5 the direct and exchange contributions to the total ^{16}O+^{16}O potential (calculated with the DDM3Y1 interaction) at incident energies ranging from 10 to 90 MeV/nucleon. As can be seen from the upper and middle parts of Fig. 5, most of the energy dependence of the HI potential is coming from the exchange term. For the nucleon-nucleus optical potential the same effect has been demonstrated earlier by Love [26] and in our recent study (see Fig. 2 from Ref. [11]). One can also see from Fig. 5 that the exchange potential is dominating at small internuclear distances, especially at low energies, which means that the density-dependent contribution from $V_{\rm EX}$ is also much stronger than that from V_D. In the surface region the overlap density decreases exponentially and the contribution of $V_{\rm EX}$ becomes comparable and even less than that of V_D. At distances $R \geq 7$ fm the total HI potential becomes dominated by the direct part only. This also explains why the simple folding model [1] has been so successful in most cases of HI scattering where the data are sensitive to the tail of the HI optical potential only. It should be noted further that the SNE effects taken into account within our folding calculations approximately exhaust the total exchange potential when the incident energy is not very low. According to the results obtained by Horiuchi [27] within the resonating group method, the SNE effects begin to have a dominating contribution with the incident energy approaching 30 MeV/nucleon. At lower energies the two- and more nucleon exchange processes might not be negligible and a rough way to take them into account in our folding calculations is to renormalize slightly the total strength of the folded potential. One finds also from our results that the higher the incident energy the less dominant the exchange potential and both the exchange

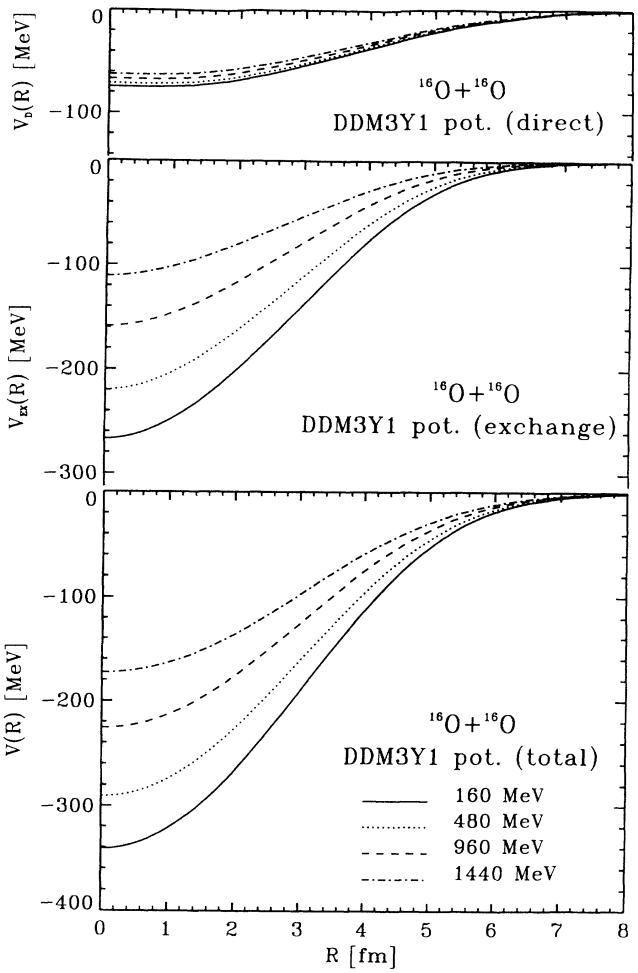

FIG. 5. The direct (upper part) and exchange (middle part) contribution to the total folded DDM3Y1 potential (lower part) for the ^{16}O+^{16}O system at incident energies ranging from 10 to 90 MeV/nucleon.

and direct potentials are of the same strength even at small distances (see dash-dotted curve in Fig. 5). Since the absolute strength of the energy-dependent exchange potential is governed to a certain extent by the chosen shape of the effective NN forces [28] [see, e.g., Eqs. (1)], the folding analyses of the scattering data over a wide energy range might impose some restriction on the effective NN interaction, i.e., an indirect inverse information on the in-medium NN forces. This is among the topics of our future study using the new version of the folding model given in the present paper.

B. ^{12}C+^{12}C system

^{12}C+^{12}C is among the most studied light HI system so far with the scattering data measured at incident energies ranging from a few and up to 200 MeV/nucleon. Very interesting are the low-energy data measured by Stokstad *et al.* [29] where the absorption has been found to be quite weak allowing the appearance of strong nuclear rainbow effects in the angular distribution [30]. A de-

tailed OM analysis of these data by Brandan *et al.* [31] has shown that the optical potentials are exceptionally transparent and can provide information on the $^{12}C+^{12}C$ interaction at very small internuclear distances. In the present paper we have performed the folding analyses for the $^{12}C+^{12}C$ data at E_{lab} = 112 and 126.7 MeV, which are not very low, so that one can still rely on the FDA adopted in our model. The results obtained with all four types of the folded potential are shown in Table II and in the upper and middle parts of Fig. 6. Following the previous OM analyses [30,31], we have assumed the volume WS shape for the imaginary potential. A slight renormalization of the real folded potentials is also allowed and the renormalization factor (N_R) is adjusted to give the best fit to the data. Besides the many-nucleon exchange effects mentioned above, which might lead to a renormalization of the folded potential, the dynamical polarization potential (ΔU) caused by the coupled-channel effects has been proven to also contribute to the real part of the optical potential. It has been shown by Sakuragi *et al.* [32] that ΔU for the $^{12}C+^{12}C$ system is surface peaked and repulsive, hence the N_R values smaller than unity can be anticipated, in general.

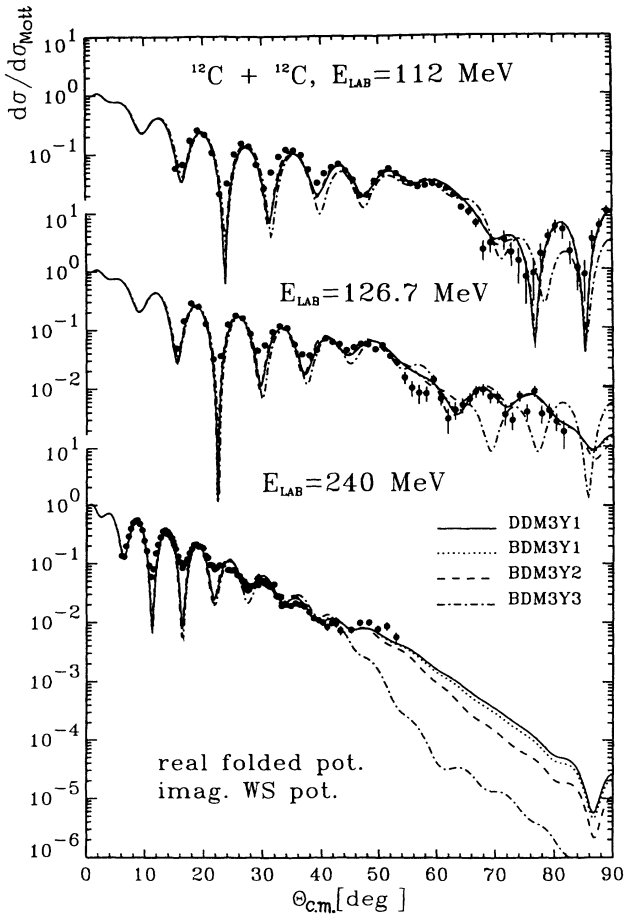

FIG. 6. The fits to the elastic $^{12}C+^{12}C$ scattering data at E_{lab} = 112, 126.7, and 240 MeV given by different types of the optical potential. The real parts of the optical potential were calculated using different density dependent versions of the M3Y interaction, while the imaginary parts were assumed to have a volume Woods-Saxon shape.

From the fits given by different types of the folded potential shown in Fig. 6 one finds that a reasonable good fit can be obtained with the DDM3Y1, BDM3Y1, and BDM3Y2 potentials. The corresponding imaginary WS potentials (Table II) are weak and quite close to those found in Refs. [30,31] which clearly show the transparency of the optical potential for the $^{12}C+^{12}C$ system at these energies. The N_R values obtained with the best-fit folded potentials are very close to unity which also indicates the weak (or cancelling) contributions of ΔU and many-nucleon exchange effects to the real optical potential. The slope and strength of the BDM3Y3 potential are quite different from those of other folded potentials, especially at small radii (as shown in Fig. 2 for the $^{16}O+^{16}O$ system). Due to this reason it is very hard to reproduce the large-angle scattering data using the BDM3Y3 folded potential, e.g., the prominent minimum in the 127 MeV data at about 60° which was specified [30] as the second Airy minimum of the nuclear rainbow, is clearly shifted by the wrong structure of the BDM3Y3 potential to larger angles (middle part of Fig. 6). It is also remarkable that values of the volume integral of the real optical potential per interacting nucleon pair J_R,

$$J_R(E) = \frac{4\pi N_R}{A_1 A_2} \int_0^\infty [V_D(E,r) + V_{EX}(E,r)]\, r^2 dr, \quad (17)$$

obtained with the first three folded potentials (see Table II), are also very close to the systematics found earlier [31], while the J_R value obtained with the BDM3Y3 potential is different from the "standard" value [31] by about 25%. The DDM3Y1, BDM3Y1, and BDM3Y2 potentials belong to the same family of the deep refractive potentials; however, with these low-energy $^{12}C+^{12}C$ data, one is still unable to find out which potential from this group is the most appropriate to describe the data.

We have considered further the elastic data for this system measured at 240 and 300 MeV by the HMI group [3,4], where a rainbow enhancement of the scattering cross section at large angles has been observed. As opposed to the data at lower energies, the small-angle parts of the scattering cross section in these cases have been measured quite accurately which allows one to determine the strength of the optical potential at the surface rather uniquely. The N_R values of different folded potentials (Table II) are mainly determined by the strength of the real potential at the surface region which in turn is fixed by the data in the diffraction region. Several data points in the refractive (rainbow) region have large error bars and influence the OM fitting procedure very little. However, the difference between different types of the folded potential at small distances shows up in the calculated cross sections at large angles, and this leads us to the best type of the folded potential which gives a reasonable description to the data in the whole angular range. From Figs. 6 and 7 one can see that the best choice of the folded potential is clearly the DDM3Y1 and BDM3Y1 ones. Even though the other two potentials (BDM3Y2 and BDM3Y3) give the χ^2 values of about the same order as the first two potentials (Table II), the description of the large-angle data given by the BDM3Y2 and BDM3Y3

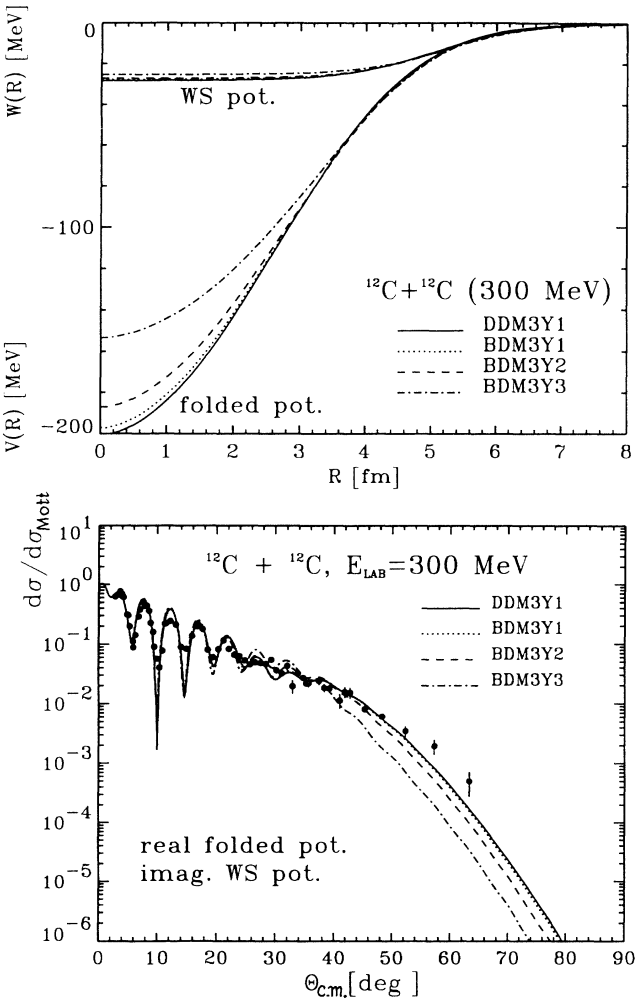

FIG. 7. The same as in Fig. 6 for the ^{12}C+^{12}C data at E_{lab} = 300 MeV (lower part) with the radial shapes of the real folded (V) and volume (W=WS) Woods-Saxon imaginary potentials used in the OM calculation (upper part).

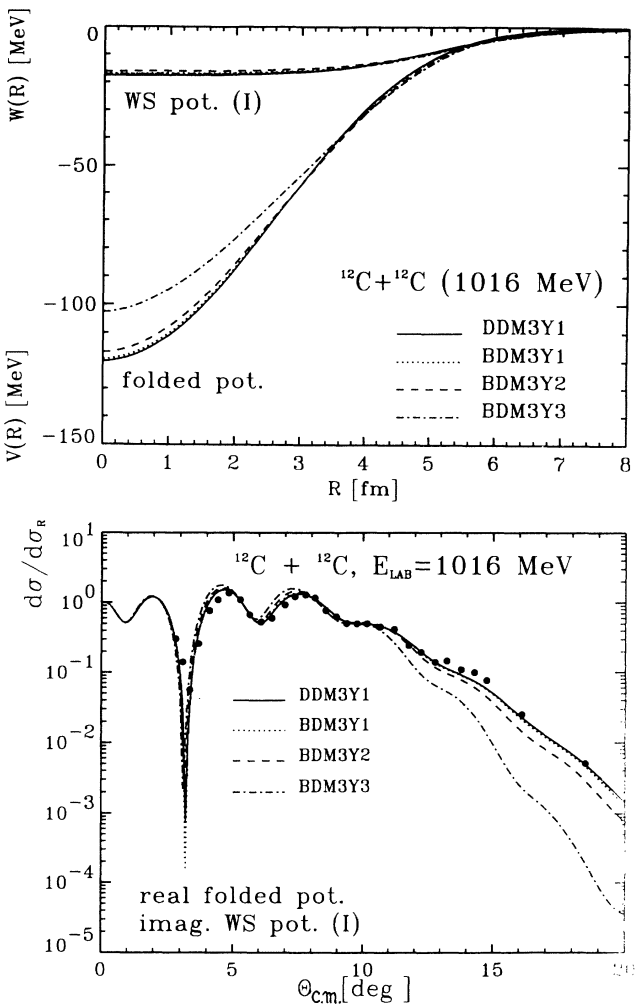

FIG. 8. The same as in Fig. 7 for the ^{12}C+^{12}C data at E_{lab} = 1016 MeV with the "weak W" set for the imaginary potential [WS(I) in Table II].

potentials is visibly worse. To illustrate the origin of this effect we have plotted in the upper part of Fig. 7 the optical potentials used in our analyses of the 300 MeV data (the real folded and WS imaginary potentials). Since the weak WS imaginary potentials are close in strength and shape, the discrepancy in the calculated cross sections at large angles is mainly due to the difference in the real folded potentials at small internuclear distances.

A detailed folding analysis has also been done for the ^{12}C+^{12}C data at E_{lab} = 1016 [33] and 1449 MeV [34]. The earlier OM analyses of these data [33,34] have implied that the data are sensitive to the real optical potential down to about 3 fm even though no clear rainbow pattern has been observed. Results of our analysis of the data at 1016 MeV are plotted in Figs. 8 and 9 with the parameters of optical potential given in Table II. For this particular case our analysis has revealed a similar ambiguity in the imaginary potential like that found earlier in Ref. [35] with the simple DDM3Y folded potential. Namely, there are two families of the WS imaginary potential: the weak one with the depth around 16 MeV and the strong one with the depth near 50 MeV. In the first case the total optical potential is rather transparent and the difference in the real folded potentials at about 3 fm (upper part of Fig. 8) is showing up in the calculated cross section. One can see that the best fit in the "weak W" case is again given by the DDM3Y1 and BDM3Y1 potentials. In the case of strong-absorptive WS potentials (see Fig. 9) all the real folded potentials give about the same fit to the data and one can see no sensitivity of the data to the real potential at small radii. The folding results obtained for the energy of 1449 MeV have the same tendency, with the existence of the "weak W" and "strong W" solutions. In view of somewhat better χ^2 values obtained with the "strong W" potentials [WS(II) in Table II], it is difficult to argue in favor of the "weak W" solutions [WS(I) in Table II] of the ^{12}C+^{12}C optical potential where one has indeed a sensitivity of the data to the real potential down to about 3 fm. Such a situation typically arises in cases where the refractive and diffractive structures are superimposed at small scattering angles. This ambiguity might be solved from a more systematic study of the accurate data at various incident energies which would allow one to extract a realistic

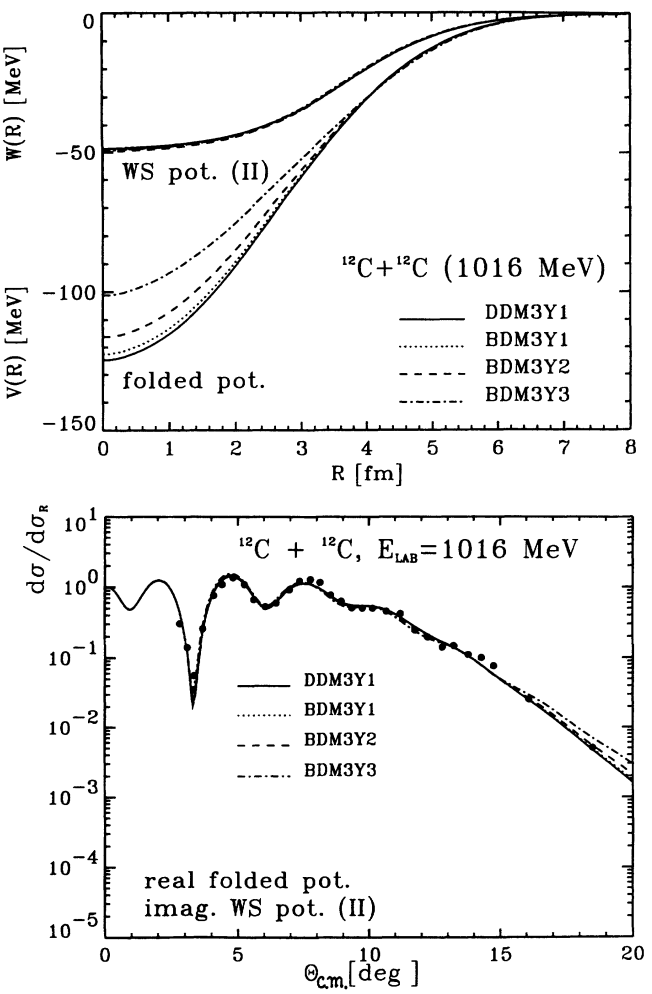

FIG. 9. The same as in Fig. 7 for the ^{12}C+^{12}C data at E_{lab} = 1016 MeV with the "strong W" set for the imaginary potential [WS(II) in Table II].

energy dependence of the imaginary potential. Unfortunately, such data are still not available, especially at high energies, except for the ones considered here [33,34]. An intuitive extrapolation of the low-energy results would support the "weak W" family which consistently gives rather transparent optical potentials for the ^{12}C+^{12}C system at all energies. We have shown that such a transparency gives some information on the ^{12}C+^{12}C potential at small distances and implies that from the 4 types of the folded potential considered here the DDM3Y1 and BDM3Y1 potentials are the most suitable ones to fit the data.

C. ^{16}O+^{16}O system

Although there are already many theoretical and experimental papers devoted to the ^{16}O+^{16}O system, new interest has arisen recently in connection with the accurate elastic data measured at E_{lab} = 350 MeV by the HMI-Group [5,36] which gave clear evidence for a nuclear rainbow. Subsequently, many OM analyses of these data were made using different kinds of the optical potential for the ^{16}O+^{16}O system [20,36–39]. In spite of certain ambiguities found in the determination of the optical potential for this case, we can now confirm [36] the sensitivity of the ^{16}O+^{16}O data at 350 MeV to the scattering potential at small distances. Encouraged by the interesting refractive effects seen at 350 MeV, some new measurements have been performed for the ^{16}O+^{16}O system at other energies [40–42]. A rather weak absorption has been found for this system which is clearly due to the double closed-shell structure of the ^{16}O nucleus. The scattering and transfer cross sections have also been measured at quite large angles where the refractive contributions are dominant [36]. In the present paper we have analysed the ^{16}O+^{16}O data at 350 MeV again as well as the new data at other energies [40–42] using all four types of the folded potential as done above in the ^{12}C+^{12}C case.

Since the data in the diffraction region have been measured very accurately, in small steps of the scattering angle, they dominantly affect the χ^2 fitting procedure. In order to keep the sensitivity of the large-angle data points to the potential, each OM fit to the ^{16}O+^{16}O data has been done in two steps. First, the uniform 10% error is assigned to all data points to find some preliminary values for N_R and the parameters of the imaginary potential as was usually done in previous OM analyses [37,38]. After a reasonable agreement with the data in the whole

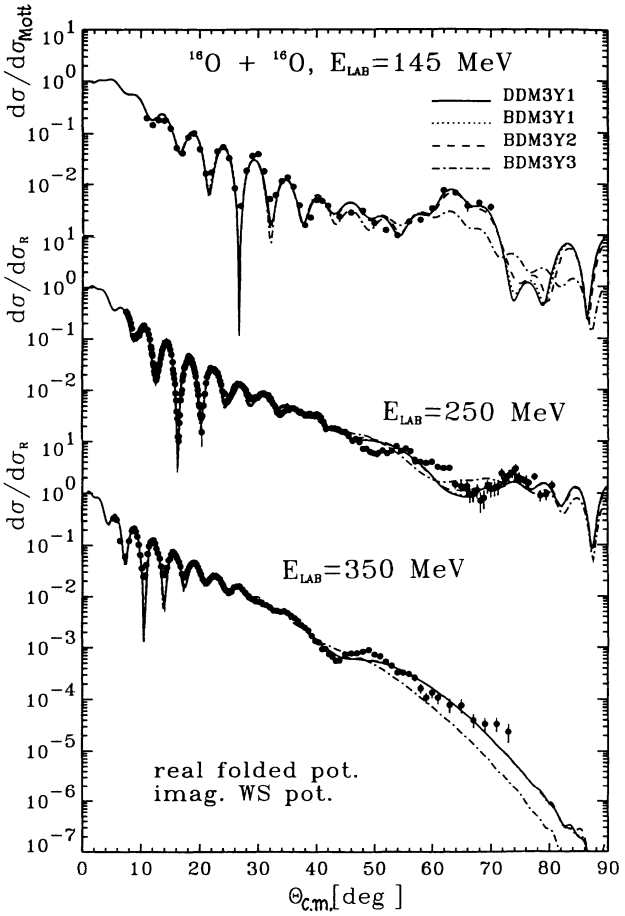

FIG. 10. The same as in Fig. 6 for the ^{16}O+^{16}O data at E_{lab} = 145, 250, and 350 MeV.

TABLE III. The same as Table II for the $^{16}O+^{16}O$ system at E_{lab} = 145–480 MeV.

Potential	N_R	$-J_R$ (MeV fm^3)	$< r_R^2 >^{1/2}$ (fm)	W_V (MeV)	R_V (fm)	a_V (fm)	σ_R (mb)	χ^2
$^{16}O+^{16}O$, E_{lab} = 145 MeV								
DDM3Y1	0.9445	339.0	4.1574	17.133	6.0028	0.6905	1693	53.4
BDM3Y1	0.9653	340.3	4.1597	17.490	5.9726	0.7011	1702	55.4
BDM3Y2	1.0154	344.4	4.1706	18.531	5.9176	0.7128	1714	59.8
BDM3Y3	1.0588	341.2	4.2075	22.601	5.8798	0.6552	1673	70.9
$^{16}O+^{16}O$, E_{lab} = 250 MeV								
DDM3Y1	0.8905	303.7	4.1650	28.498	5.6184	0.7368	1762	46.0
BDM3Y1	0.9099	304.7	4.1675	28.429	5.6318	0.7349	1763	48.4
BDM3Y2	0.9510	306.3	4.1788	28.360	5.6600	0.7299	1767	57.0
BDM3Y3	0.9866	301.8	4.2160	28.270	5.7002	0.7161	1762	74.6
$^{16}O+^{16}O$, E_{lab} = 350 MeV								
DDM3Y1	0.9218	299.4	4.1728	31.628	5.6099	0.6534	1642	40.2
BDM3Y1	0.9435	300.9	4.1754	31.430	5.6366	0.6470	1642	41.2
BDM3Y2	0.9942	304.8	4.1870	30.980	5.6999	0.6330	1645	43.4
BDM3Y3	1.0369	301.7	4.2248	31.914	5.7048	0.6301	1652	48.6
$^{16}O+^{16}O$, E_{lab} = 480 MeV								
DDM3Y1	0.8520	259.8	4.1838	32.675	5.3984	0.7434	1657	6.7
BDM3Y1	0.8741	261.6	4.1866	32.517	5.4274	0.7377	1660	6.9
BDM3Y2	0.9116	262.2	4.1986	32.988	5.6948	0.6030	1588	10.5
BDM3Y3	1.0224	278.9	4.2370	33.521	5.5213	0.7502	1735	10.6

angular range is obtained, the final OM fit is done with the experimental uncertainties of the data starting from the parameters of the preliminary search. Thus we could avoid the "unrealistic" sets of the optical potential which sometime give even smaller χ^2 values but visibly worse descriptions to the data at large angles. The results given by different types of the real folded potential using the simple volume WS shape for the imaginary potential are given in Table III and plotted in Fig. 10 (the fit to the preliminary data at 480 MeV [42] is done to have a guide in the energy dependence of the $^{16}O+^{16}O$ potential only). Similarly to the results obtained above for the $^{12}C+^{12}C$ system, the deep DDM3Y1 and BDM3Y1 potentials turn out to be the most relevant ones among the four types of the folded potential to reproduce the data over the whole angular range, and the BDM3Y3 potential is again too shallow in the center and thus gives a wrong description to the data at large angles. The renormalization of the real folded potentials in these cases is around 0.9, giving the J_R values of the real optical potential (Table III) very close to those from the energy dependence of the $^{16}O+^{16}O$ potential proposed by Kondo and co-workers [37,40] which in turn is consistent with the results of the dispersion relation and the analyses of the low-energy resonances in the $^{16}O+^{16}O$ system.

To improve the agreement of the calculated cross sections with the data in the large-angle (refractive) region, we have also included into the imaginary potential a surface term [the last term in Eq. (16)] which has been proven necessary [20,36] in reproducing the data at 350 MeV with the real folding-type potential. The real folded potentials are kept fixed as given in Table III in order to see the effects coming from the imaginary potential used in our folding analyses. While the inclusion of the surface (WSD) term does not improve the fit at E_{lab} = 145 MeV, the fit to the data at 250, and especially at 350 MeV, becomes much better with the WSD term. The improved results for the energies 250 and 350 MeV are given in Table IV and plotted in Figs. 11 and 12. Such a WS+WSD combination of the imaginary potentials simply keeps the absorption at the surface strong enough to reproduce the diffractive part of the scattering data while the absorption at small distances becomes weaker (see upper part of Fig. 12) giving rise to a broad rainbow maximum in the elastic cross section. From Figs. 11 and 12 one can also see that the inclusion of the WSD term does not much improve the fit given by the BDM3Y3 real potential. A renormalization of about 10% of the real folded potential (see N_R values from Tables III and IV) is mainly fixed by the data points at small angles and the relative difference in the shape of different folded potentials remains practically the same (compare Fig. 2 and the upper part of Fig. 11 for the 250 MeV case). Thus the best fit to the large-angle data is given by the most relevant type of the folded potential available. Our preliminary analysis [11] of the 350 MeV data using about the same real folded potentials as those in this paper with the fixed renormalization N_R = 1 has also favored the DDM3Y1 and BDM3Y1 potentials as the most realistic ones.

Different OM analyses of the data at 350 MeV [36–38] have shown that the broad maximum near 50° can be identified as a remnant of the primary rainbow (with the first Airy minimum around 44°). This rainbow structure can be reproduced if the real optical potential is deep enough to belong to the group of refractive potentials (type A from Ref. [37] or the folding-type potentials [36]). With the new data measured at 145 and 250 MeV it is of interest to study the evolution of the rainbow

TABLE IV. The same as Table II for the $^{16}O+^{16}O$ system at E_{lab}=250 and 350 MeV with the imaginary potential assumed to be a sum of a volume WS term and a surface WSD term as given in Eq. (16).

Potential	N_R	W_V (MeV)	R_V (fm)	a_V (fm)	W_D (MeV)	R_D (fm)	a_D (fm)	σ_R (mb)	χ^2
$^{16}O+^{16}O$, E_{lab} = 250 MeV, Imag. WS+WSD pot.									
DDM3Y1	0.8905	36.641	4.7915	0.9062	3.5230	5.8309	0.4268	1822	37.4
BDM3Y1	0.9099	37.876	4.7038	0.9219	3.9878	5.8064	0.4267	1829	37.2
BDM3Y2	0.9510	38.528	4.6464	0.9313	5.1053	5.7267	0.4231	1831	37.6
BDM3Y3	0.9866	39.836	4.6109	0.9355	5.6530	5.7518	0.4012	1835	41.6
$^{16}O+^{16}O$, E_{lab} = 350 MeV, Imag. WS+WSD pot.									
DDM3Y1	0.9218	25.265	5.7554	0.6488	7.9655	4.7371	0.3637	1634	39.8
BDM3Y1	0.9435	25.429	5.7578	0.6481	7.4643	4.7473	0.3823	1637	40.6
BDM3Y2	0.9942	25.929	5.7612	0.6458	6.2634	4.8143	0.4240	1645	42.3
BDM3Y3	1.0369	26.304	5.7692	0.6309	4.5614	4.9566	0.5031	1644	51.5

pattern with increasing incident energy. A very careful study in this direction has been made for the $^{12}C+^{12}C$ system by McVoy and Brandan [30] where they show a smooth shifting of the Airy minima towards small scattering angles as the energy increases. To avoid the Mott interference in the elastic cross section at large angles for the identical $^{16}O+^{16}O$ system, we have perfomed the *unsymmetrized* OM calculations of the elastic $^{16}O+^{16}O$ cross sections at 145, 250, and 350 MeV using the best-fit folded potential (DDM3Y1) with the optical potential parameters given in Table III (for the energy of 145 MeV) and Table IV. From the results shown in Fig. 13 one finds that the minimum seen at $\Theta_{c.m.} \simeq 54°$ in ex-

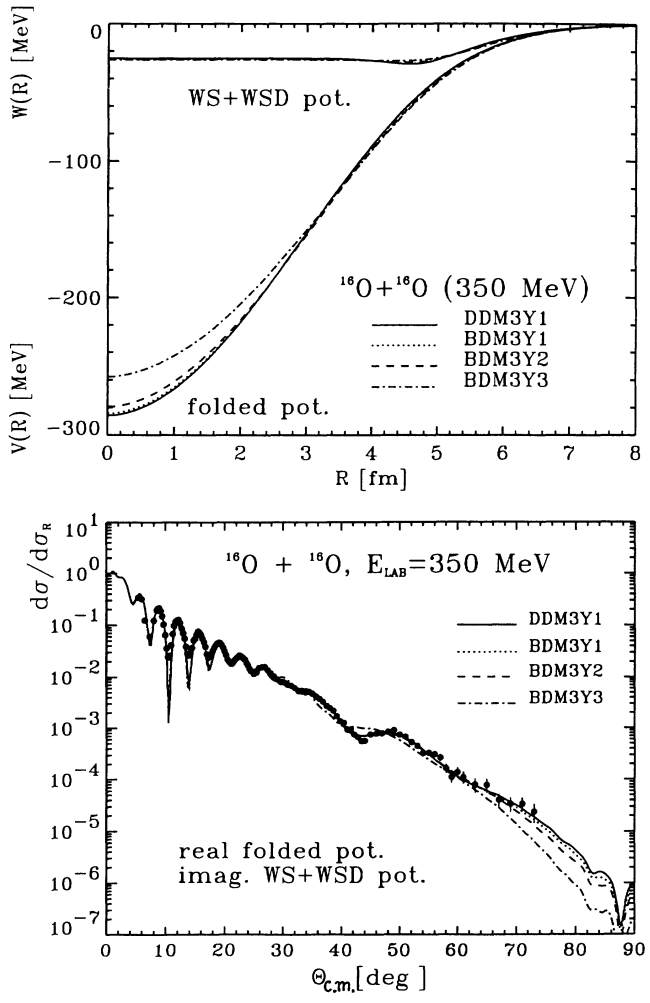

FIG. 11. The same as in Fig. 6 for the $^{16}O+^{16}O$ data at E_{lab} = 250 MeV (lower part) with the radial shapes of the real folded (V) and "volume+surface" (W=WS+WSD) Woods-Saxon imaginary potentials used in the OM calculation (upper part).

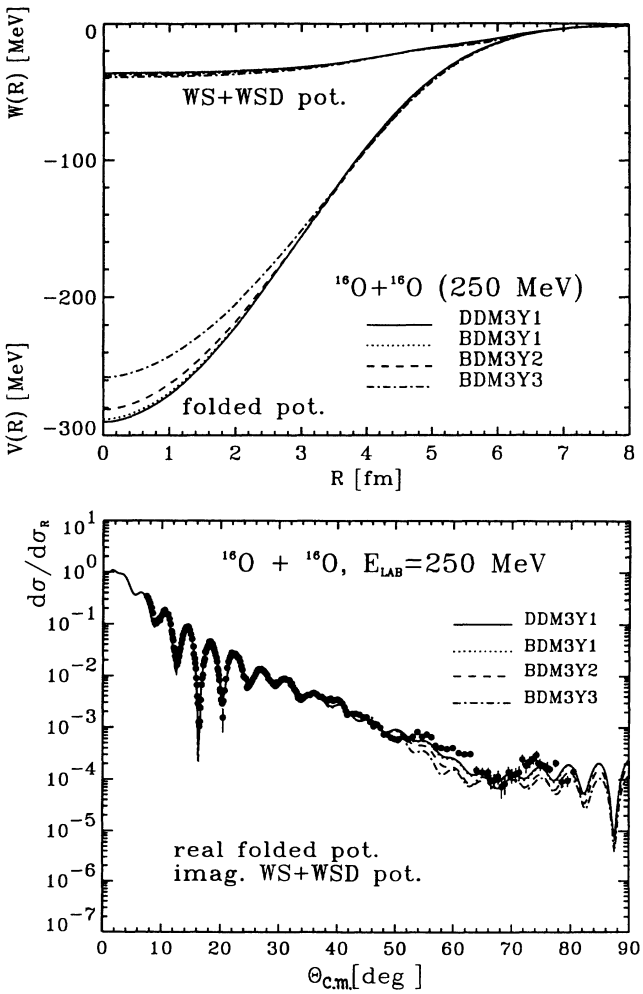

FIG. 12. The same as in Fig. 11 for the $^{16}O+^{16}O$ data at E_{lab} = 350 MeV.

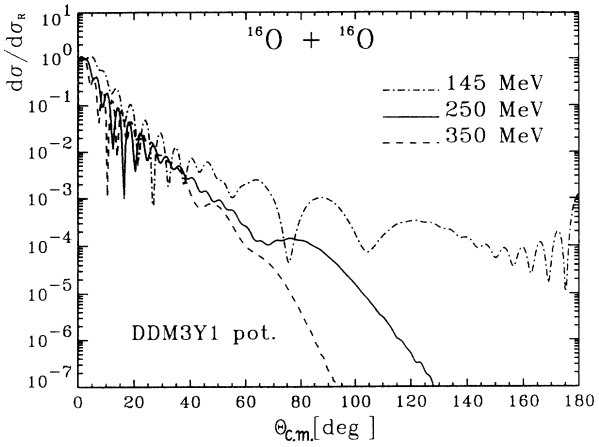

FIG. 13. The unsymmetrized OM calculations for the $^{16}O+^{16}O$ system at E_{lab} = 145, 250, and 350 MeV using the best-fit DDM3Y1 folded potential (see details in Sec. III C).

perimental data at 145 MeV is the third Airy minimum generated by the deep DDM3Y1 folded potential. This is consistent with the III Group of the optical potential for $^{16}O+^{16}O$ at 145 MeV suggested in Ref. [40], which also gives the J_R values ($\simeq$ 330 MeV) close to that predicted by the realistic energy dependence [37] mentioned above. The first Airy minimum is moving from beyond 100° at 145 MeV to around 66° and 44° at 250 and 350 MeV, respectively. It is remarkable that the broad rainbow maximum preceding the first Airy minimum for the energy of 250 MeV (solid curve in Fig. 13) can still be seen in the scattering data up to about 80° (lower part of Fig. 11) with some small oscillations caused by the Mott interference occurring at larger angles. At 350 MeV the width of this rainbow shoulder becomes smaller with the first Airy minimum moved to $\Theta_{c.m.} \simeq 44°$, closer to the diffraction region. From the results shown here we can deduce that the energy of 300 MeV would be the most optimal one to have a broad rainbow scattering pattern for the $^{16}O+^{16}O$ system not much affected either by the Mott interference at large angles or by the diffraction at small angles.

The present results and those reported in Refs. [37,38, 40] allow one to conclude that the best-fit folded potential belongs to the family of the deep refractive potentials (A type in Refs. [37,38] or III type in Ref. [40]) which consistently produce the evolution of the Airy oscillation with the energy. Our new version of the folding model seems to deliver a reliable real HI optical potential at different energies which gives us confidence to use the DDM3Y1 (or BDM3Y1) potential to predict the scattering cross section at the energies not yet measured. We would also like to emphasize that the persistence of Airy-like minima in the new elastic $^{16}O+^{16}O$ data [40,41] further supports the rainbow interpretation of the observed elastic-scattering data.

D. $^{16}O+^{12}C$ and $^{16}O+^{28}Si$ systems

Before drawing some systematic conclusions on the energy- and density-dependent folded potential, we would like to briefly discuss the results of our folding analyses of the $^{16}O+^{12}C$ and $^{16}O+^{28}Si$ data at somewhat higher energies [43–45] than those measured so far for the $^{16}O+^{16}O$ system. Even though there is no rainbow pattern observed in these cases, the $^{16}O+^{12}C$ data show some departure from the diffractive oscillation pattern which might be sensitive to the nucleus-nucleus potential at small radii [35]. The $^{16}O+^{12}C$ data at 1503 MeV, e.g., has been shown to be sensitive to the real optical potential at distances of 3–6 fm [46] while the "strong absorption" radius ($D_{1/2}$) for this system is at about 6.2 fm. The elastic cross sections obtained with different types of the folded potential for these cases are plotted in Figs. 14 and 15 and the optical potential parameters are given in Table V. As in the $^{12}C+^{12}C$ cases at high energies considered in Sec. III B, we have also found two different families of the imaginary potential for the $^{16}O+^{12}C$ data at 1503 MeV (the fit to the $^{16}O+^{12}C$ data at 608 MeV using our real folded potentials seems to prefer the "weak W" solution only). From Fig. 14 one can see again that the best description to the $^{16}O+^{12}C$ data in the whole angular range is given by the DDM3Y1 and BDM3Y1

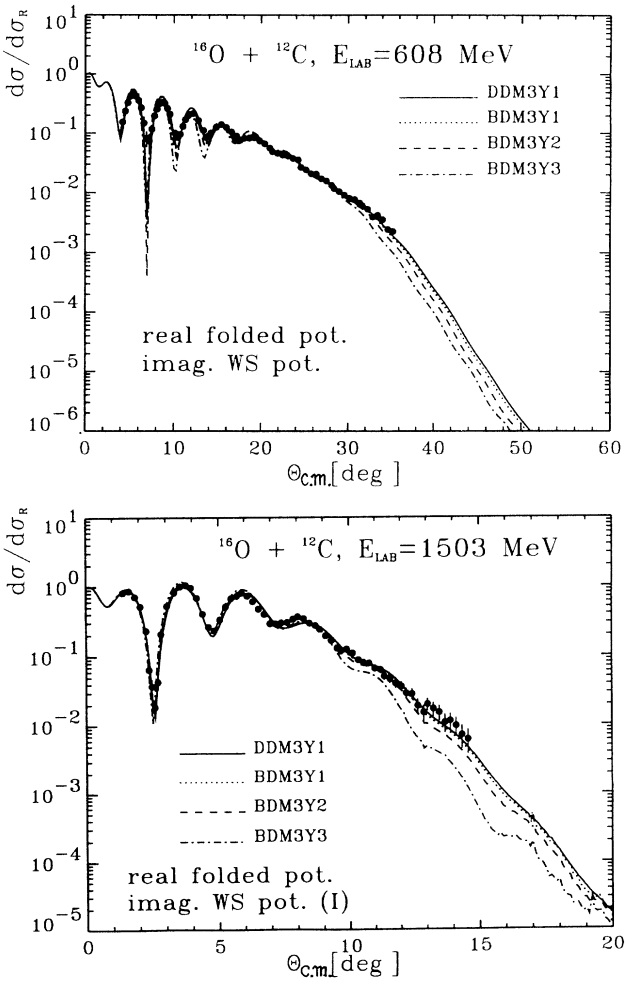

FIG. 14. The same as in Fig. 6 for the $^{16}O+^{12}C$ data at E_{lab} = 608 and 1503 MeV obtained with the "weak W" set for the imaginary potential [WS(I) in Table V] at the energy of 1503 MeV.

TABLE V. The same as Table II for the elastic $^{16}O+^{12}C$, and ^{28}Si scattering at E_{lab}=608 and 1503 MeV.

Potential	N_R	$-J_R$ (MeV fm^3)	$< r_R^2 >^{1/2}$ (fm)	W_V (MeV)	R_V (fm)	a_V (fm)	σ_R (mb)	χ^2
$^{16}O+^{12}C$, E_{lab} = 608 MeV								
DDM3Y1	0.8341	233.0	4.0218	25.528	5.3465	0.6109	1350	7.0
BDM3Y1	0.8503	232.3	4.0277	24.996	5.3831	0.6092	1357	8.2
BDM3Y2	0.8894	231.3	4.0475	23.758	5.4772	0.6097	1381	11.7
BDM3Y3	0.9505	230.1	4.1026	21.554	5.6744	0.6251	1451	17.5
$^{16}O+^{12}C$, E_{lab} = 1503 MeV, Imag. WS (I) pot. (Effective lab. energy=1454.27 MeV, ^{16}O mass=16.294 and ^{12}C mass=12.389)								
DDM3Y1	0.8699	164.5	4.1204	16.240	5.6629	0.7741	1323	9.0
BDM3Y1	0.8905	164.4	4.1272	15.767	5.7248	0.7688	1331	7.8
BDM3Y2	0.9413	164.9	4.1492	14.731	5.8717	0.7528	1347	6.2
BDM3Y3	1.0234	166.3	4.2071	13.078	6.1233	0.7291	1376	10.4
$^{16}O+^{12}C$, E_{lab} = 1503 MeV, Imag. WS (II) pot. (Effective lab. energy=1454.27 MeV, ^{16}O mass=16.294 and ^{12}C mass=12.389)								
DDM3Y1	1.0913	206.3	4.1204	44.629	4.8051	0.6097	1178	13.4
BDM3Y1	1.1068	204.4	4.1272	44.258	4.7992	0.6142	1179	13.2
BDM3Y2	1.1398	199.7	4.1492	43.261	4.7822	0.6272	1180	12.2
BDM3Y3	1.1798	191.7	4.2071	41.312	4.7362	0.6600	1186	9.7
$^{16}O+^{28}Si$, E_{lab} = 1503 MeV (Effective lab. energy=1478.34 MeV, ^{16}O mass=16.643 and ^{28}Si mass=28.372)								
DDM3Y1	0.8940	170.5	4.5855	68.250	5.2639	0.7741	1744	5.7
BDM3Y1	0.9042	169.0	4.5913	68.096	5.2458	0.7829	1750	5.7
BDM3Y2	0.9250	165.4	4.6101	67.484	5.2084	0.8027	1762	5.6
BDM3Y3	0.9472	159.4	4.6593	65.364	5.1786	0.8257	1774	5.7

potentials only, provided the absorption at 1503 MeV is weak. The fits to the $^{16}O+^{12}C$ and $^{16}O+^{28}Si$ data at 1503 MeV obtained with the "strong W" solutions for the imaginary potential are shown in Fig. 15. In these cases all the real folded potentials give about the same description to the data, i.e., one finds no sensitivity to the real optical potential at small radii when the absorption is strong in this radial region. All the renormalization factors of the real folded potential N_R obtained for the $^{16}O+^{12}C$ system at 1503 MeV with a "strong W" imaginary potential [WS(II) set in Table V] are greater than unity. This is somewhat out of the systematic behavior (Tables II–V) found for the best-fit real folded potential (around 0.9 and depends weakly on the energy), a fact that might favor the weak-absorptive [WS(I)] set of the optical potential for the $^{16}O+^{12}C$ system at 1503 MeV. Note that for the heavier $^{16}O+^{28}Si$ system we could find no "weak W" solution which indicates that this system is a strong absorbing one and the data are no longer sensitive to the potential at subsurface distances.

The results presented here have shown again that the weak absorption (or the transparency of the optical potential) found for different light HI systems enables one to test the real optical potential down to quite small internuclear distances. Among the four types of the real folded potential being tested in our analyses, the DDM3Y1 and BDM3Y1 potentials are shown to be the most realistic ones.

E. Energy dependence of the real HI potential

As has been discussed repeatedly in different folding analyses, the renormalization factor N_R of the folded potential should not deviate strongly from unity. The closer to 1 the N_R factor the more realistic the model used for the nucleus-nucleus potential [1]. From the other side, the folded potential is only the first-order term of the HI potential and higher-order terms, e.g., the dynamical polarization correction ΔU, contribute to both the real and imaginary parts of the HI optical potential. Such a contribution to the real potential is shown to be in many cases repulsive and surface peaked [32] and the N_R values smaller than 1 might be considered as reasonable. All the N_R values obtained with the best-fit (DDM3Y1) folded potential from our analyses of the elastic ^{16}O and ^{12}C scattering data are plotted vs the incident energy in the upper part of Fig. 16. We have also deduced the N_R factors of the DDM3Y1 potential for the $^{16}O+^{40}Ca$ system at 139.6 and 214.1 MeV by scaling the strength of the DDM3Y1 potential to the best-fit values [1] at the "strong absorption" radii ($D_{1/2}$) found for this system. One can see from the upper part of Fig. 16 that the N_R factor depends very weakly on the energy and varies around a value of 0.9. The same behavior can be found for the BDM3Y1 potential (see Tables II–V). Consequently, the intrinsic energy dependence arising from the exchange effects [see Eqs. (6) and (7)] and the weak explicit energy dependence [$g(E)$ factor in Eq. (2)] introduced into the effective NN interaction [11] are indeed the main sources of the total energy dependence of the real HI optical potential.

The values of the volume integral of the real folded potential per interacting nucleon pair J_R are plotted in the lower part of Fig. 16. With the incident energy increasing from about 10 to 120 MeV/nucleon, the J_R values decrease smoothly from about 340 to 150 MeV fm^3.

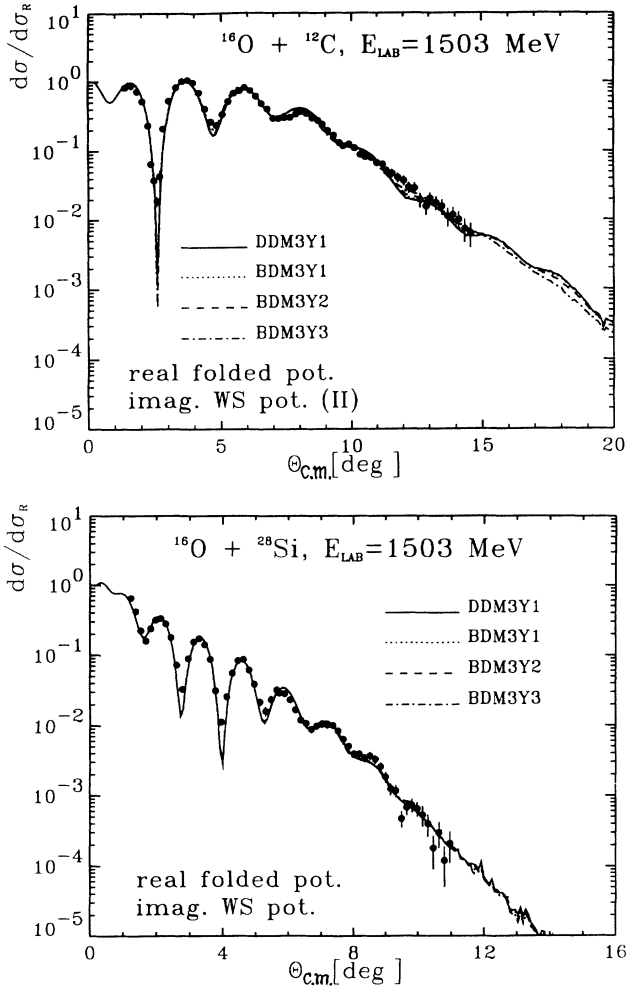

FIG. 15. The same as in Fig. 6 for the ^{16}O+^{12}C and ^{28}Si data at E_{lab} = 1503 MeV obtained with the "strong W" set for the imaginary potential [WS(II) in Table V] for the ^{16}O+^{12}C system.

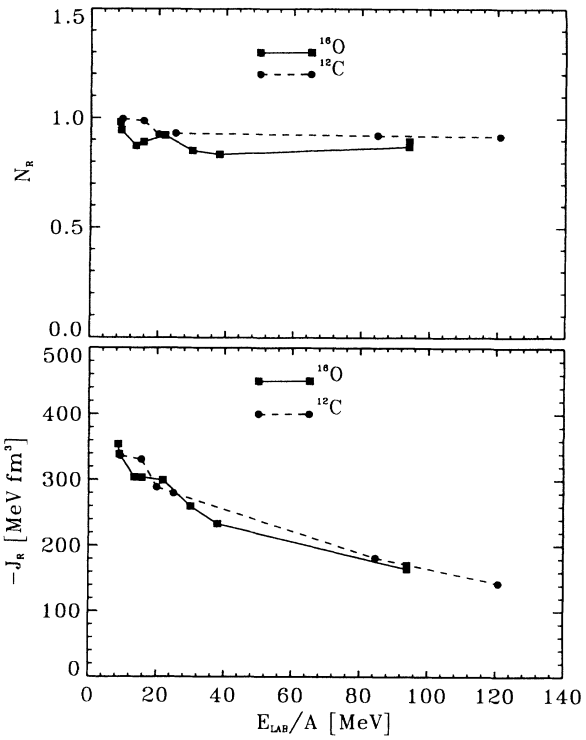

FIG. 16. The energy dependence of the renormalization factor N_R (upper part) and the volume integral J_R (lower part) of the DDM3Y1 potential deduced from the folding analyses of the elastic ^{16}O and ^{12}C scattering data at energies up to 120 MeV/nucleon.

These results agree quite well with a realistic energy dependence of the J_R values deduced from the earlier OM analyses of the elastic ^{12}C [31] and ^{16}O [37] scattering. From this discussion we can conclude that the energy dependence of the real HI optical potential is predicted quite well by the new version of the folding model given in the present paper.

F. The cold nuclear EOS

Finally, we would like to stress the influence of different choices of the cold EOS (Fig. 1) on the results of our folding analyses. We have shown above that the refractive scattering data, which in most cases require a rather transparent optical potential, are very sensitive to the real HI potential at small radii. Such data imply that among the four types of the folded potential considered in our analyses, the DDM3Y1 and BDM3Y1 potentials are the most relevant ones. This means that the density dependences DDM3Y1 and BDM3Y1 introduced into the original M3Y interaction are the most realistic ones. Since the connection between a density-dependent effective NN interaction and the EOS of the cold nuclear matter is straightforward [11], we may conclude from our analyses of the refractive HI scattering that the EOS corresponding to the nuclear compressibility $K \simeq$ 150–210 MeV might be the most realistic for the cold nuclear matter. This preliminary conclusion on the nuclear EOS is in an agreement with some models of supernova explosion [47] where a value of $K \simeq$ 200 MeV or lower is suggested. Note that a method of extracting the K value from the excitation energies of the observed giant monopole resonances was widely applied [48], but it has been shown that a unique value for K cannot be extracted and any value from 200 to 350 MeV can be deduced. Many attempts to determine the nuclear EOS have been undertaken via the study of the high-energy central HI collisions where one hopes to deduce from the measured transverse flows or various particle (and nuclear-fragment) spectra some information on the EOS. Different semimicroscopic transport models [25,49] have been used successfully in reproducing such data. The basic input for such a calculation is some effective two-body interaction (Skyrme-type forces) with parameters fixed to give a soft ($K \simeq$ 200 MeV) or a hard ($K \simeq$ 380 MeV) EOS of the cold nuclear matter. Due to the uncertainties in the experimental data as well as in different inputs used in these calculations, the results obtained so far remain inconclusive concerning the nuclear EOS. Moreover, the high-density nuclear matter formed

during the compression stage of a central HI collision is quite hot, with the temperature in the range of 50–100 MeV [50]; and the EOS of the *heated* nuclear matter is of course different from that of the *cold* nuclear matter. In this sense, our study of refractive HI scattering within the present model (using the input for the *cold* EOS to study the *cold* nuclear matter) consistently gives a clear answer to the question about the cold EOS. A more precise determination of the K value for the cold nuclear matter with the inclusion of more data on the $^{16}O+^{16}O$ scattering is now in preparation.

IV. SUMMARY

The double-folding model has been generalized for the calculation of the real HI optical potential using the new density-dependent versions of the M3Y interaction [11] with parameters chosen to consistently reproduce the basic nuclear matter properties and the energy dependence of the nucleon optical potential. The exchange part of the folded potential is evaluated within the local density formalism, with the SNE effects taken into account exactly.

Detailed folding analyses are performed for the elastic ^{12}C and ^{16}O scattering data at energies from about 10 to 120 MeV/nucleon using different types of the real folded potential which have been calculated with different density-dependent M3Y interactions. It has been shown that most of the considered $^{12}C+^{12}C$ and $^{16}O+^{16}O$ data favor a rather transparent optical potential which has a sufficiently weak-absorptive imaginary potential. In these cases the large-angle scattering data can be interpreted as being of the refractive nature and they are sensitive to the real optical potential at small internuclear distances. Such a sensitivity implies a stronger restriction on the shape and strength of the folded potential, so that one can extract the most realistic potential from different types of the folded potential used in the analyses.

The DDM3Y1 and BDM3Y1 potentials have been found to be the most appropriate in the family of the folded potentials. These two types of the real folded potential are calculated within the new model using the density-dependent interactions which in turn can be used to microscopically generate [11] a cold nuclear EOS which is rather soft and has the compressibility $K \simeq 150$–210 MeV. These results provide, therefore, an evidence that the cold nuclear matter is most probably governed by a soft EOS.

The best-fit folded potentials, renormalized by a factor N_R of about 0.9, reproduce reasonably well the energy dependence of the real optical potential for ^{12}C and ^{16}O scattering found in previous OM analyses. These potentials belong to the family of the deep refractive potentials which consistently describe the Airy-like structures at large scattering angles observed in the $^{12}C+^{12}C$ and $^{16}O+^{16}O$ scattering data at different energies.

Systematic analyses of more data as well as a sophisticated microscopic calculation of the imaginary potential are highly desirable to confirm the transparency of the optical potential for the $^{12}C+^{12}C$ and $^{16}O+^{16}O$ systems found in our analyses. This would further support the rainbow interpretation of the large-angle scattering data as well as our preliminary conclusion on the EOS of the cold nuclear matter.

ACKNOWLEDGMENTS

We thank Ray Satchler for valuable comments and continuing interest in the present study, Y. Sugiyama for providing the $^{16}O+^{16}O$ data at 145 MeV in tabular form, and H. Clement and K.W. McVoy for helpful discussions during their visits to HMI Berlin. The useful correspondence with M. E. Brandan is also acknowledged.

[1] G.R. Satchler and W.G. Love, Phys. Rep. **55**, 183 (1979).
[2] D.A. Goldberg, S.M. Smith, H.G. Pugh, P.G. Roos, and N.S. Wall, Phys. Rev. C **7**, 1938 (1973); D.A. Goldberg, S.M. Smith, and G.F. Burdzik, *ibid.* **10**, 1362 (1974).
[3] H.G. Bohlen, M.R. Clover, G. Ingold, H. Lettau, and W. von Oertzen, Z. Phys. A **308**, 121 (1982).
[4] H.G. Bohlen, X.S. Chen, J.G. Cramer, P. Fröbrich, B. Gebauer, H. Lettau, A. Miczaika, W. von Oertzen, R. Ulrich, and Th. Wilpert, Z. Phys. A **322**, 241 (1985).
[5] E. Stiliaris, H.G. Bohlen, P. Fröbrich, B. Gebauer, D. Kolbert, W. von Oertzen, M. Wilpert, and Th. Wilpert, Phys. Lett. B **223**, 291 (1989); HMI Annual Report 1989, HMI-B-482, p. 50.
[6] G. Bertsch, J. Borysowicz, H. McManus, and W.G. Love, Nucl. Phys. **A284**, 399 (1977).
[7] A.M. Kobos, B.A. Brown, P.E. Hodgson, G.R. Satchler, and A. Budzanowski, Nucl. Phys. **A384**, 65 (1982); A.M. Kobos, B.A. Brown, R. Lindsay, and G.R. Satchler, *ibid.* **A425**, 205 (1984).
[8] A.K. Chaudhuri, D.N. Basu, and B. Sinha, Nucl. Phys. **A439**, 415 (1985); A.K. Chaudhuri and B. Sinha, *ibid.* **A455**, 169 (1986).
[9] Dao T. Khoa, Nucl. Phys. **A484**, 376 (1988); Dao T. Khoa, A. Faessler, and N. Ohtsuka, J. Phys. G **16**, 1253 (1990).
[10] W.G. Love and L.W. Owen, Nucl. Phys. **A239**, 74 (1975); M. Golin, F. Petrovich, and D. Robson, Phys. Lett. B **64**, 253 (1976).
[11] Dao T. Khoa and W. von Oertzen, Phys. Lett. B **304**, 8 (1993).
[12] H. Müther, Prog. Part. Nucl. Phys. **17**, 97 (1986); R. Brockmann and R. Machleidt, Phys. Lett. B **149**, 283 (1984).
[13] J.P. Jeukenne, A. Lejeune, and C. Mahaux, Phys. Rev. C **16**, 80 (1977).
[14] X. Campi and A. Bouyssy, Phys. Lett. B **73**, 263 (1978).
[15] P. Ring and P. Schuck, *The Nuclear Many-body Problem* (Springer-Verlag, New York, 1980), p. 542.
[16] R. Baltin, Z. Naturforsch. **27A**, 1176 (1972).
[17] M. Trefz, A. Faessler, and W.H. Dickhoff, Nucl. Phys.

A443, 499 (1985); N. Ohtsuka, R. Linden, A. Faessler, and F.B. Malik, *ibid.* **A465**, 550 (1987).
[18] M. El-Azab Farid and G.R. Satchler, Nucl. Phys. **A438**, 525 (1985).
[19] Dao T. Khoa and O.M. Knyazkov, Z. Phys. A **328**, 67 (1987); Dao T. Khoa and O.M. Knyazkov, Yad. Fiz. **47**, 1246 (1988) [Sov. J. Nucl. Phys. **47**, 793 (1988)].
[20] Dao T. Khoa, W. von Oertzen, A. Faessler, M. Ermer, and H. Clement, Phys. Lett. B **260**, 278 (1991).
[21] H. Abele and G. Staudt, Phys. Rev. C **47**, 742 (1993); H. Abele, Ph.D. thesis, University of Tübingen (1992).
[22] R.M. DeVries and M.R. Clover, Nucl. Phys. **A243**, 529 (1975); J.E. Poling, E. Norbeck, and R.R. Carlson, Phys. Rev. C **13**, 648 (1976).
[23] M.H. Macfarlane and S.C. Pieper, Argonne National Laboratory Report No. ANL-76-11 (1978).
[24] M. El-Azab Farid and G.R. Satchler, Phys. Lett. B **146**, 389 (1984).
[25] J. Aichelin, Phys. Rep. **202**, 233 (1991).
[26] W.G. Love, Nucl. Phys. **A312**, 160 (1978).
[27] H. Horiuchi, in *Trends in Theoretical Physics*, edited by P.J. Ellis and X.C. Tang (Addison-Wesley, Tokyo, 1990), Chap. 13, p. 277.
[28] T. Wada and H. Horiuchi, Phys. Rev. C **38**, 2063 (1988).
[29] R.G. Stokstad, R.M. Wieland, G.R. Satchler, C.B. Fulmer, D.C. Hensley, S. Raman, L.D. Rickertsen, A.H. Snell, and P.H. Stelson, Phys. Rev. C **20**, 655 (1976).
[30] K.W. McVoy and M.E. Brandan, Nucl. Phys. **A542**, 295 (1992).
[31] M.E. Brandan, M. Rodriguez-Villafuerte, and A. Ayala, Phys. Rev. C **41**, 1520 (1990).
[32] Y. Sakuragi, M. Yahiro, and M. Kamimura, Prog. Theor. Phys. Suppl. **89**, 136 (1986).
[33] M. Buenerd, A. Lounis, J. Chauvin, D. Lebrun, Ph. Martin, G. Duhamel, J.C. Gondran, and P. de Saintignon, Nucl. Phys. **A424**, 313 (1984).
[34] J.Y. Hostachy, M. Buenerd, J. Chauvin, D. Lebrun, Ph. Martin, J.C. Lugol, L. Papineau, P. Roussel, N. Alamanos, J. Arvieux, and C. Cerruti, Nucl. Phys. **A490**, 441 (1988).
[35] M.E. Brandan and G.R. Satchler, Nucl. Phys. **A487**, 477 (1988).
[36] H.G. Bohlen, E. Stiliaris, B. Gebauer, W. von Oertzen, M. Wilpert, Th. Wilpert, A. Ostrowski, Dao T. Khoa, A.S. Demyanova, and A.A. Ogloblin, Z. Phys. A **346**, 189 (1993).
[37] Y. Kondo, F. Michel, and G. Reidemeister, Phys. Lett. B **242**, 340 (1990).
[38] M.E. Brandan and G.R. Satchler, Phys. Lett. B **256**, 311 (1991); M.E. Brandan, K.W. McVoy, and G.R. Satchler, *ibid.* **281**, 185 (1992).
[39] L. Allen, L. Berge, C. Steward, K. Amos, H. Fieldeldey, H. Leeb, R. Lipperheide, and P. Fröbrich, Phys. Lett. B **298**, 36 (1993).
[40] Y. Sugiyama, Y. Tomita, H. Ikezoe, Y. Yamanouchi, K. Ideno, S. Hamada, T. Sugimitsu, M. Hijiya, and Y. Kondo, Phys. Lett. B **312**, 35 (1993).
[41] H.G. Bohlen *et al.* (unpublished).
[42] G. Bartnitzky *et al.* (unpublished).
[43] M.E. Brandan, A. Menchaca-Rocha, M. Buenerd, J. Chauvin, P. de Saintignon, G. Duhamel, D. Lebrun, P. Martin, G. Perrin, and J.Y. Hostachy, Phys. Rev. C **34**, 1484 (1986).
[44] P. Roussel, N. Alamanos, F. Auger, J. Barrette, B. Berthier, B. Fernandez, L. Papineau, H. Doubre, and W. Mittig, Phys. Rev. Lett. **54**, 1779 (1985).
[45] P. Roussel, J. Barrette, F. Auger, B. Berthier, B. Fernandez, J. Gastebois, A. Gillibert, L. Papineau, W. Mittig, D. Disdier, B. Lott, V. Rauch, F. Scheibling, C. Stephan, and L. Tassan-Got, Phys. Lett. B **185**, 29 (1987).
[46] A.M. Kobos, M.E. Brandan, and G.R. Satchler, Nucl. Phys. **A487**, 457 (1988).
[47] E.D. Baron, J. Cooperstein, and S. Kahana, Nucl. Phys. **A440**, 744 (1985).
[48] J.P. Blaizot, Phys. Rep. **64**, 171 (1980); A. van der Woude, Prog. Part. Nucl. Phys. **18**, 217 (1987); S. Shlomo and D.H. Youngblood, Phys. Rev. C **47**, 529 (1993).
[49] G.F. Bertsch and S. Das Gupta, Phys. Rep. **160**, 198 (1988); W. Cassing, V. Metag, U. Mosel, and N. Nitta, *ibid.* **188**, 363 (1990).
[50] Dao T. Khoa, N. Ohtsuka, A. Faessler, M.A. Matin, S.W. Huang, E. Lehmann, and Y. Lotfy, Nucl. Phys. **A542**, 671 (1992).